J. Condensed Matter Nucl. Sci. 4 (2011) 93–105

Research Article

Impact of an Applied Magnetic Field on a High Impedance Dual Anode LANR Device

Mitchell R. Swartz *

JET Energy Inc., Massachusetts, USA

Abstract

This paper reports on the impact of an applied magnetic field intensity on LANR solution electrical resistance and an analysis of its role in metal deuteride loading and LANR performance. A dual anode PHUSOR®-type Pd/D_2O/Au LANR device was driven at its optimal operating point, with two electrical current sources; to drive, and examine by 4-terminal electrical resistance, the loaded PdD_x cathode. An applied magnetic field ~0.3 T increases the LANR solution's electrical resistance ~10–17% with a time constant in minutes. The incremental resistance increase to an applied H-field is greatest at low loading current. The incremental resistance increase from an applied H-field is greatest with the applied H-field perpendicular to the driving electrical field (E-field) intensity. The modified LANR deuteron loading rate equation indicates that an applied magnetic field intensity increases deuteron loading in a LANR system by the increasing solution resistance and limiting undesired gas evolving reactions.

Keywords: Deuterium, Deuterons, Excess heat, Excess power gain, Flux, Lattice assisted nuclear reactions, Loading, Metamaterials, Nanostructures, Optimal operating point, Palladium
PACS: 28.52.-s, 72.15.-v, 75.30.-m

1. Lattice Assisted Nuclear Reactions

Lattice assisted nuclear reactions (LANR) use hydrogen-loaded alloys to enable near room temperature deuterium fusion and other nuclear reactions [1–49] using deuterons as fuel. Technologies which increase LANR excess energy production include thermal power spectroscopy [4], optimal operating point operation [1,3,4,24], the use of high electrical impedance solutions [3,4], metamaterial shapes [1,32] and nanostructures [1,37,60]. Correctly driven, LANR metamaterial nanostructured devices exhibit excess heat, excess heat flow, and non-thermal near infrared (NT-NIR) emission linked to both [34]. LANRs generated ("excess") power densities range from ~7 (1989 announcement) to 80–10,000 W/cm^3, today. Over time, the magnitude of generated excess power yields significant excess heat, and material changes which are wrought on the electrode, such as volcano-like pits [8,18,19].

At LANRs "core" are deuterons which are tightly packed into binary ("highly loaded") metals and metallic nanostructures by an applied electric field or elevated gas pressure which supply deuterons in heavy water or gaseous deuterium.

*E-mail: mica@theworld.com

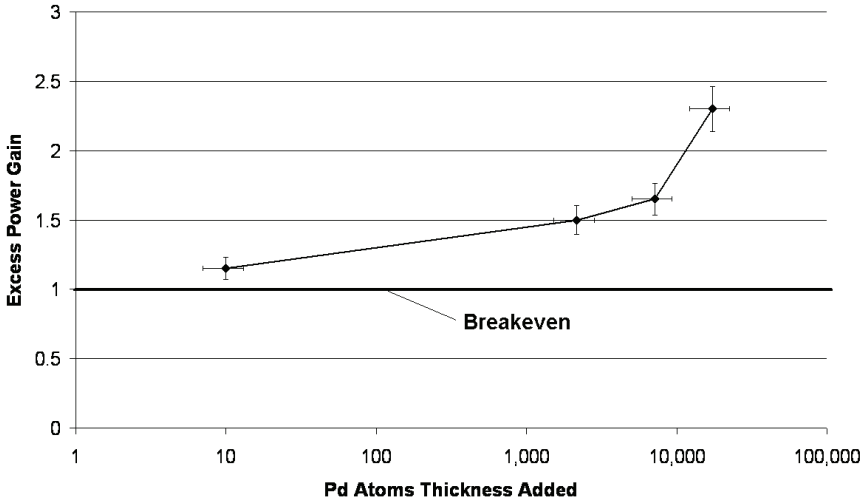

Figure 1. Excess Heat Correlated With Pd Codepositional Thickness Such high impedance metamaterial nanostructured LANR devices have shown power gains more than 200% and short term power gains to ∼8000% [1,2], compared to input energy and to input energy transferred to conventional dissipative devices.

With control of LANR devices by precise nanostructure fabrication, metamaterial shape selection using high impedance ("High-*Z*") PHUSOR®-type LANR devices in very high electrical resistivity (the real part of the complex impedance, with units of ohms) D_2O, control of D-flux and post D-loading flux, there is a higher likelihood of achieving LANRs impressive energy gain, and with time integration – excess heat, with fairly good reproducibility.

Dual anode PHUSOR® LANR devices (DAP) use two anodes. The first is for preparation of the codepositional surface and solution, and the second is used to drive the active surface [37,68]. Investigations of DAP LANR devices (Fig. 1) have demonstrated that nanostructures are important in LANR with sizes involving circa 10 atoms or more in size. Corroboration of this fact includes experimental results in codeposition [25] and non-thermal near IR (NT NIR; Fig. 3) emissions [34]. The curve in Fig. 1 demonstrates with experimental evidence that LANR excess heat is correlated with the size of the Pd–D nanostructures, which can be considerable (Fig. 2). Figure 1 shows the monotonic increase in excess heat from LANR as the codepositional layer was increased in size over loaded palladium, apparently beginning with nanosize structures in temperature (degrees centigrade, delta-*T*) for both the ohmic thermal control and the DAP PHUSOR® type LANR device. The input power normalized delta-*T* was used to compare the LANR and control (ohmic) systems over varying input powers. Sites 1 and 2 represent two sites within the active LANR cell. Site 3 was located at the ohmic (joule) control, consisting of a carbon resistor. In Fig. 2, over time, electrical power was first delivered to the control and then to the LANR device. The important point is that Fig. 2 demonstrates an LANR power gain of ∼8000%.

By imaging near infra-red, Fig. 3 shows a distribution of LANR activity over the surface of an LANR device, consistent with nanostructures. It shows the emission of near-IR from the electrodes when excess heat is only observed and the active electrodes operated at their optimal operating point (OOP; [1,2,57]), and then the nonthermal near IR emission (NT-NIR) is linked and specific to the LANR devices' excess heat production and not its physical temperature [34]. This results from the temperature-related shift from hot fusion's penetrating ionizing radiation to LANR's skin-depth-locked infrared radiation [50]. Unlike hot fusion or plasma systems, bremsstrahlung radiant power density falls from 0.05 to 0.28 (hot fusion) to $1.4–8.1\times10^{-10}$ for LANR. The delivered X-ray dose at 1 m decreases by incredible 18–

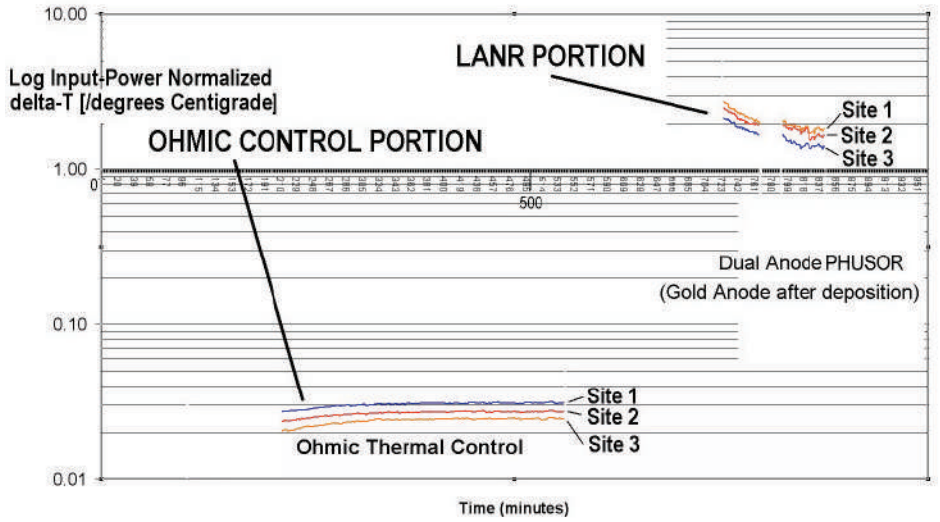

Figure 2. Input power normalized delta-*T* curves for DAP PHUSOR® LANR Fig. 2 shows the transient output of one DAP (Pd^*/D_2O-$Pd(OD)_2$/Au Dual Anode PHUSOR®-type) LANR device. The graph shows the input power-normalized change.

23 orders of magnitude from 3.1 × 1019 Grays (hot fusion) to $\sim 2 \times 10^{-4}$ Grays for LANR. In addition, the temperature difference also causes the output spectrum of the Bremsstrahlung radiation to be shifted to the near infra-red, consistent with the NIR emission of LANR systems at their OOP. Figure 3 shows three visible and nearinfrared (NIR) views of a DAP codeposition PHUSOR®-type LANR device in heavy water. The platinum anode is seen in the background. The DAP PHUSOR® is located in both images ($\sim$7.7 mM $Pd(OD)_2$). The inset view is in ordinary light, the other two (from a slightly different angle of observation) are in the near infrared (NIR). The image on the left precedes ("off"), and the one on the right is after activation and generation of excess heat of the PHUSOR®-type LANR system.

Given these LANR reactions, there has been much interest in the application of magnetic field intensities to LANR

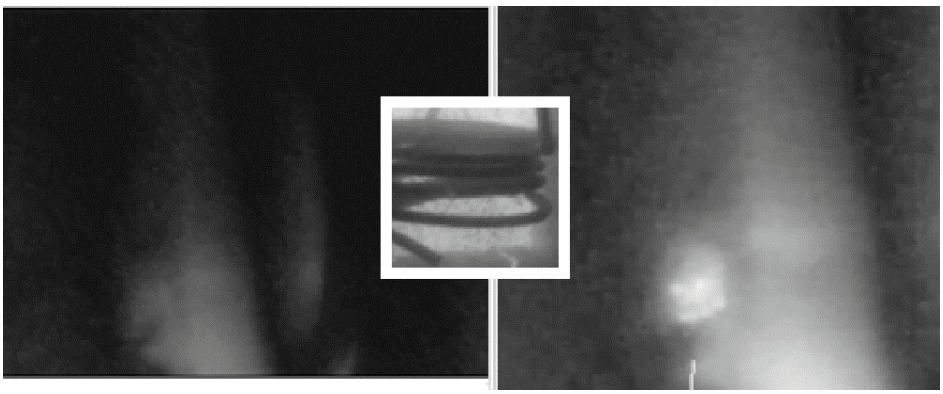

Figure 3. Near-infrared images of DAP LANR cell, before and after activation, with close-up of cathode in visible light (inset) – after Swartz (2010; Ref. [34]).

systems. Dr. Pamela Mosier-Boss et al. at SPAWAR have reported morphology changes on the cathode with an applied magnetic field intensity [19]. For reasons that will become clear in the Interpretation section, because of the complex impact of laser irradiation of LANR cathodes upon solution electrical resistance and power gain [33], we elected to first report on the effect of those applied magnetic field intensities on LANR solution's electrical conductivity because that material parameter is decisive in the success of LANR systems.

2. Experimental Details

The six terminal LANR codepositional high impedance device used here was a DAP LANR device (Dual anode PHUSOR®-Type LANR device; Pd/D_2O, Pd$(OD)_2$/Pt–Au). It contain nanostructures whose preparation, assembly, and driving is complicated and described elsewhere [1,2, 3,4,34,35,37]. The LANR cathodes were prepared from 99.98+% Pd [Alfa Aesar, Ward Hill, MA], 1.0 mm diameter, $\sim 4-7$ turns on a spiral of $\sim$1.3 cm diameter, with a gap separation from the anode arranged in a Pd/D_2O/Pt or Pd/D_2O/Au configuration (Pt 99.998%). The solution was 7.7 mM Pd$(OD)_2$ in low paramagnetic high electrical resistivity heavy water (deuterium oxide, low paramagnetic, 99.99%, Cambridge Isotope Laboratories, Andover MA) with no additional electrolyte. For the DAP devices, palladium is laid down from a sacrificial anode upon the surface of a palladium cathode. Then, the palladium anode is removed, and replaced by a gold wire anode to stop the further laying down of further palladium nanostructure upon the palladium cathode. Interestingly, we have reported a new phenomenon during codepositional layering of the DAP cathode. This consists of a dynamic instability oscillation, an electrohydrodynamic Rayleigh–Bernard instability associated with the layering. The time constant was circa 15 min per cycle, but this was irregular, with three to five cycles occurring in a 60 min period. Contamination remains a major problem, with excess heat devastatingly quenched by decreasing electrical resistance of the solution [2–4] the effects on the cathode can be minimized. Contaminants appear from both electrode and container degradation and leeching, from atmospheric contamination, and after temperature cycling. These all inexorably, unintentionally, add to the electrolytic solution decreasing the level of deuteron loading, the rate of loading as well, and the maximum heat producing activity. The heavy water is hygroscopic, therefore kept physically isolated from the air by seals, including several layers of Parafilm M (American National Can, Menasha, WI) and paraffin. All leads near the solution were covered with electrically insulating tubes (medical grade silicone, Teflon, or proprietary materials) used to electrically isolate wires. We continue to avoid chlorine or chloride because of possible explosions from visible light ignition susceptibility, which results because the activation energy with chlorine is only $\sim$17 μJ.

The loading of the palladium from the heavy water, and driving of the reactions through the two electrodes within the reaction container was obtained by controlled electric current source, or a Keithley 225 at low input, with $\pm$1% accuracy. Electrical voltage sources included HP/Harrison 6525A for transsample potentials up to 3000 V ($\sim \pm$0.5% accuracy). All connections isolated, when possible, with Keithley electrometers for computer isolation. To allow 4-terminal electrical resistance measurements within the loaded PdD_x cathode, a first Keithley 225 electric current source was used to drive the cell, and load the cathode, and then a second Keithley 225 electric current source was used to drive the electrical current portion of the four terminal electrical resistivity measurement of the palladium. The data from voltage, current, temperatures at multiple sites of the solution, and outside of the cell, the 4-terminal measurement of the cathode's internal electrical conductivity, additional calibration thermometry and other measurements were sampled at 0.20 Hz, usually 1 Hz, 22+ bits resolution (Omega OMB-DaqTemp, voltage accuracy 0.015$\pm$0.005 V, temperature accuracy $<$0.6°C) and recorded by computed DAQ. To minimize quantization noise, 1 min moving averages were sometimes made. The noise power of the calorimeter is in the range of $\sim$1–30 mW. The noise power of the Keithley current sources is $\sim$10 nW. Input power is defined as VI. There is no thermo-neutral correction in denominator. Therefore, the observed power is a lower limit. The instantaneous power gain [power amplification factor (nondimensional)] is defined as $P_{\text{out}}/P_{\text{in}}$, as calibrated by at least one electrical joule control (ohmic resistor) and time integrated for validation. The excess energy, when present, is defined as $(P_{\text{output}} - P_{\text{input}}) \times$ time.

The amount of output energy is interfered from the heat released producing a temperature rise, which is then compared to the input energy. Temperature measurements are made by specialized electrically insulated thermocouples [(accuracy ±0.8 K, precision ±0.1 K), RTD and other sensors. Probes were calibrated by Omega IcePoint Cell and core temperatures were maintained by feedback control using a Yellow Spring Thermal Controller Model 72 (bandwidth of 0.2 K) within a Honeywell water circulation zone controlled room (±2.5 K). Thermocouples and other temperature sensors decorated the periphery of the cell, and a multicompartment calorimeter was used. There was an additional heat-flow probe at the periphery outside of the core. To minimize contamination, the majority of temperature measurements were outside of the inner core container. Calorimetry is augmented by heat flow measurement, electricity production using thermoelectrics, and LANR-driven motors. Outputs are calibrated by ohmic (thermal) controls, and dual ohmic (calorimeter) controls, to evaluate, and certify possible excess heat. Additional calibration has included adequate Nyquist sampling, time-integration, thermal ohmic controls, waveform reconstruction, noise measurement, and other techniques [2–4]. During the experiment, an attempt was made to determine, first, the impact of the direction of the electrical current used for the 4-terminal measurements along the cathode, and second, the impact of the direction of the applied magnetic field intensity obtained from neodymium magnets. The stationary applied magnetic field intensity was circa 0.3 T, and the field was directed either parallel or perpendicular to the applied electric field intensity used to load and drive the LANR device.

3. Results -– Magnetic Fields

Within the DAP (Dual Anode PHUSOR®-type $Pd/D_2O/Au$ LANR) device, solution resistances ranged from 800,000 Ω initially to ∼5000 Ω. The 4-terminal cathodes measurements of electrical resistance of the loaded metal ranged from ∼50 to 120 mΩ. For the DAP device, the excess heat was measured as the thickness increased to ∼17,000 atoms deep (Fig. 1). At that time, the solution was 7.7 mM $Pd(OD)_2$, and the open circuit voltage, V_{oc}, used to determine the effectivity of LANR [2,3], was 1.46 V. The Pd^*/D_2O-$Pd(OD)_2$/Au PHUSOR®-type system has an initial cell resistance of circa 868 kΩ, which fell to circa 48.3 kΩ upon final preparation.

For the DAP (Dual Anode PHUSOR®-type $Pd/D_2O/Au$ LANR device), applying a static magnetic field to the LANR system increased the solution's electrical resistance by 10–17%. This is shown in Fig. 4. The increase in solution electrical resistance was greatest at lower levels of electrical driving of the LANR system (1 mA vs. 10 mA). The increase in solution electrical resistance was greatest when the applied magnetic field was perpendicular to the driving electrical field intensity.

Figure 5 shows the time course of the changes to the magnetic field intensity. The time constant was on the order of minutes.

4. Interpretation – Deuteron Fluxes in LANR

An applied magnetic field in LANR can effect the resistance of the solution, and as will be shown below, that increased resistance can increase metal deuteride loading. Relevant to this analysis were our past studies which examined the impact of laser irradiation on LANR cathodes and reported, in 2003, that it decreases the solution electrical resistance and increases LANR excess heat, but decreases LANR power gain.

Deuteron flux is a key issue in LANR. Nernst calculations of the activities of the electrolyte [51,52] adjacent to a metal electrode have been applied to LANR to derive distributions of deuterium in palladium and the solution. However, because the LANR systems are not at equilibrium, such Nernst calculations are generally not applicable [53,54]. By contrast, unaffected by non-equilibrium, the quasi-1-dimensional (Q1D) model of deuteron loading [53] has been used to analyze deuteron populations and deuteron flow. It has foundation in the known dielectric properties of materials

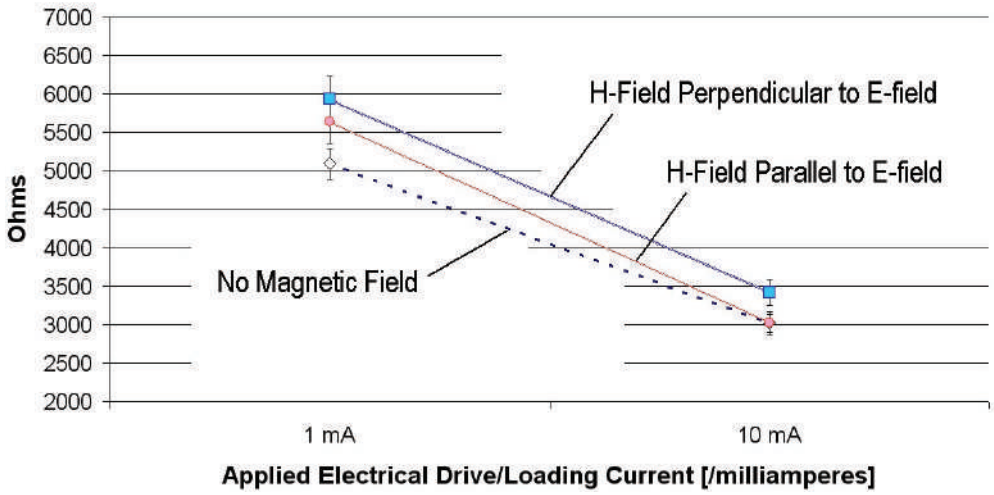

Figure 4. Effect of applied H-field on DAP PHUSOR®- LANR device's solution electrical resistance.

[55] and continuum electromechanics [56], and has generated the deuteron-flux equations which explain the reason for LANR's difficulty – and the road to success.

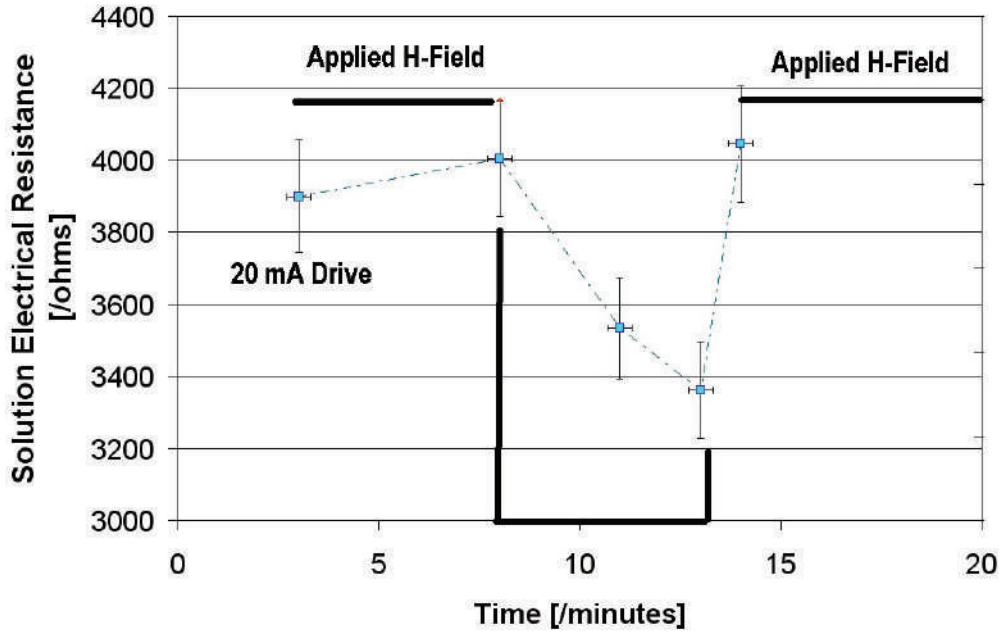

Figure 5. Time course of solution electrical resistance after change of applied H-field.

Several different deuteron populations and fluxes must be distinguished [57] at the surface of the low hydrogen-overvoltage palladium, with its surface highly populated with atomic, diatomic (D_2), and bulk-entering deuterons [1,32]. The deuteron fluxes are seen on the left of Fig. 6, which is a schematic, simplified, representation of the anode, solution, and a portion of the cathode along with five types of deuteron fluxes involved in LANR.

The deuteron fluxes are deuteron cationic flow in the solution (J_D), and the four types of deuteron flux in the loaded palladium cathodic lattice (J_E, J_G, J_F, and J_{IP}). The latter are the entry of deuterons to the metal lattice ("loading", J_E), movement to gas (D_2) evolution ("bubble formation", J_G), intrapalladial deuteron flux (J_{IP}) flow through the metal (generated by metamaterials), and an extremely tiny loss by the desired fusion reactions (J_F). There is conservation of deuterons with the exception of a loss (J_F) to all putative fusion reactions, which are extremely small, when present.

As Fig.6 shows, cationic deuteron flux (J_D) brings deuterons to the cathode surface to create a cathodic fall and double layer before the electrode surface. It begins far from the cathode surface, in the deuterium oxide (heavy water) located between the electrodes, where the deuterons are tightly bound to oxygen atoms as D_2O. In the absence of significant solution convection, the flux of deuterons (J_D) results from diffusion down concentration gradients and electrophoretic drift by the applied electric field [53,54,56,58].

$$J_D = -B_D \frac{d[D(z,t)]}{dz} - \mu_D [D(z,t)] \frac{d\Phi}{dz}, \tag{1}$$

J_D depends on deuteron diffusivity (B_D) and electrophoretic mobility (D), and the applied electric field intensity. At any molecular site across the heavy water solution, the applied electrical energy is a tiny fraction compared to $k_B T$, so the deuterons migrate by drift ellipsoids of L- and D-deuteron defects in the applied electric field creating a ferroelectric inscription [58,59]. This D-defect conduction/polarization process augments other charge carriers, ionic drift, space charge polarization and clathrates. The resultant D-defect migration produces a "cathodic fall" of deuterons and a E-field contraction so that most of the voltage drop is at the interface in front of the electrode surface. This concentration polarization may produce very large local electric field intensities, possibly ranging from 10^4 to 10^7 V/cm [53,54].

From the concentration polarization of deuterons before the cathode, at the inner boundary of the double layer, intermolecular deuteron transfer from the heavy water solution to the metal surface is controlled and limited by electron-limited transfer, which leaves an atomic deuteron on the metal surface. The transfer mechanisms to the palladium surface are driven by infrared vibrations and microwave rotations [33,59], creating a solution photosensitivity which produces a photo-activated increase of excess energy and loss of power gain [33].

On the metal surface, the plethora of atomic deuterons either enter the metal ("are loaded") forming a binary alloy [60–67], or remain on the surface, or form diatomic deuterium gas bubbles (D_2). As a result, palladium has its

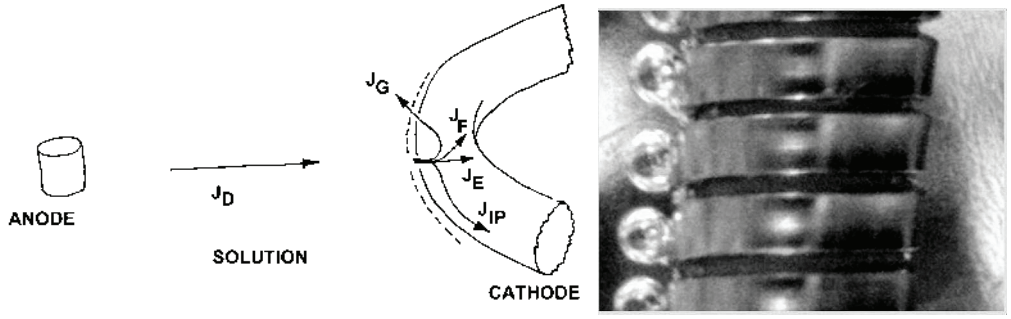

Figure 6. Deuteron Fluxes in LANR (a) Left – Schematic of deuteron fluxes, from solution to loaded metal. (b) Right – Close-up of active LANR cathode (after Swartz 2006, Ref. [17]).

surface populated with atomic (D) and diatomic deuterium (D_2). Any deuterons which enter the metal are electrically neutralized ('dressed') by a partial electronic cloud, shielding their charge (in a Born–Oppenheimer approximation) [37]. The deuterons drift along dislocations and through the lattice and its vacancies, falling from shallow to deeper located binding sites. There is competing obstruction by ordinary hydrogen and other materials at interfaces and grain boundary dislocations. The gas bubbles (D_2) are undesirable producing low dielectric constant layers in front of the electrode, obstructing the electrical circuit. As derived elsewhere [53], after solving the partial differential equations, and using conservation of mass, and numerically dividing each deuteron flux (J_E, J_G, and J_F) by the local deuteron concentration to yield the first-order deuteron flow rates, k_E, k_G, and k_F (with units of cm/s, respectively), Eq. (2) is the deuteron flux equation of LANR. Numerically, ke might be in the range of 0.5–30 μA, and the concentration of (D) is circa 50 M.

$$\kappa_e = \mu_D E - (\kappa_g + \kappa_f). \tag{2}$$

Equation (2) is the deuteron loading rate equation. It relates cathodic deuteron gain from the applied electric field to the loss of deuterons from gas evolution and fusion, and teaches many things. The deuteron loading rate equation shows that the deuteron gain of the lattice [through the first order loading flux rate (k_E)] is dependent upon the applied electric field *minus* the flux rate losses of deuterons from gas evolution (k_G) and fusion (k_F). The deuteron loading rate equation, Eq. (2), reveals that desired LANR reactions are quenched by electrolysis, which is opposite conventional "wisdom" that LANR is 'fusion by electrolysis'. Equation (2) also heralds that LANR can be missed by insufficient loading, contamination (effecting k_E, by protons or salt) and by the evolution of D_2 gas, which all inhibit the desired LANR reactions [53,1,2] and leading to the optimal operating point manifolds. This quenching is of prime importance.

Equation (2) can be modified to Eq. (3), the modified deuteron loading rate equation, by substituting into it the Einstein relation. There are many important lessons for LANR.

$$k_e = \frac{B_D q V}{L[k_B T]} - (\kappa_g + \kappa_f). \tag{3}$$

The first term now has geometric and material factors. B_D is the diffusivity of the deuteron. $k_B T$ is the Boltzmann's constant and temperature. q is the electronic charge, and V is the driving applied voltage. Most importantly, dominating the first term is the ratio of two energies (the applied electric energy organizing the deuterons divided by $k_B T$, thermal disorder). This energy ratio is decisive in controlling the deuteron loading flux in palladium – and thus LANR. Successful LANR experiments reflect the 'war' between applied electrical energy which is organizing the deuterons versus their randomization by thermal disorganization.

The second term includes the first-order deuteron loss rates by gas evolution and the desired fusion process(es). The minus sign means that the second term heralds that competitive gas evolving reactions at the metal electrode surface can destroy (quench) the desired reactions. The first-order loading flux rate constant (k_E) is dependent upon the applied electric field intensity minus the first-order gas loss rate constant resulting from gas (D_2) evolution at the cathode (k_G). This implication is exactly opposite conventional "wisdom" that LANR is 'fusion by electrolysis' [1–4]. LANR can be missed by insufficient loading, contamination (effecting k_E, by protons or salt), and by the evolution of D_2 gas, which all inhibit ("quench") the desired LANR reactions [3,4]. Note that Eq. (3) with the Einstein relation is similar to some flux equations from solid state physics, so there is the question of similarity of deuterons and their holes in Pd to holes and electrons in semiconductor materials.

5. Interpretation – Impact on Loading Rate

We believe the applied magnetic field intensity directly changes the loading rate of deuterons in to a metal deuteride. The following explains the reasons, and derives the equations demonstrating the relationship. Consider the role of

cathodic photo-irradiation in LANR. In addition to entry into the skin depth layer of the metal, a part of the impact is due to reflection off the cathode back into the double layer. Deuteron injection into the palladium increases (activation energy of ∼14 kcal per mol) from microwave rotation and IR vibration for the intermolecular transfer of deuterons to the Pd [33]. Hagelstein, Letts and Cravens [11,12] have also reported both single and dual photon impacts on cathodes as increasing excess heat. As we reported, there is a small and reproducible photo-incremental increase in both the power gain and in the observed excess heat from the coherent irradiation of the cathode, even when heating effects of the beam were included in the calibration. Near the OOP, the optical irradiation increased the excess power from 84.7±10 to 95.5±12 mW. For ∼250 mW input electrical power, the irradiation increased the excess power from 79.8±7.6 to 93.3±6.3 mW. Beyond the OOP, the impact of coherent non-ionizing radiation upon the cathode is small compared to dark heat production (power gain 1.49±0.005 in the dark, 1.50±0.005 for the laser irradiation, for input power levels which produce 400 mW excess heat). Incremental photoinduced excess power was observed only in the presence of a functioning active loaded cathode. This photoinduced excess power may be a lower limit. Issues of good optical path geometry, angle of penetration, active irradiated cathodic area, possible double layer interactions, interference with low dielectric constant bubbles formed and skin depth penetration remain relevant and suggest that the actual impact of laser irradiation may be greater.

We discovered that the effects are partially extra-cathodic. Therein lies the "rub". Even though there is an incremental photo-thermoelectric increase in excess heat production changing the net excess power from 1.7 to 1.8±0.1 W, with optical irradiation of the cathode and surrounding solution, there is an additional change. Irradiation of the cathode necessarily results in irradiation of the solution and a photoinduced decrease in the Pt/D_2O/Pd electrical resistance which increased the input electrical power dissipated (not excess). Optical irradiation of the cathodic volume and surrounding solution produces a photoinduced decrease in the effective cell-solution electrical resistance (55–51 kΩ). This increases the input electrical power for the same applied voltage. Because of the relationship between power gain (non-dimensional), excess power and input electrical power (watts), there follows a photoinduced decrease of the power gain, which is noticeable at higher input electrical power levels (2.4–2.3, for 1.3 W input).

This paradoxical decrease in the power gain heralds conduction/polarization pathways which lead away from some desired reactions. Exactly why this occurs can be understood by analysis of the modified loading flux equation. Examination of the LANR loading rate equations reveals that there are at least two ways the applied magnetic field can interact in the solution, through the ordering energy ratio and diffusivity of deuterons at the surface (first term), and through the solution resistance (second term).

Assuming a Faradaic efficiency for gas formation of ξ_g per electron, an electric current I, and accounting for the Faraday ratio to the mole, F, then

$$K_g \approx \frac{\xi_g I}{FA[D^+]}. \tag{4}$$

Substituting the electrical admittance with electrical conductivity with geometric factors, yields

$$K_g \approx \frac{\xi_g \sigma_{D_2O} V}{FL[D^+]}. \tag{5}$$

As a result, the modified LANR loading rate equation becomes

$$k_e \cong \frac{B_D q V}{L k_B T} - \frac{\xi_g \sigma_C V}{FL[D^+]}. \tag{6}$$

The term σ_C/L can be replaced by $1/AR$ (A is the area, R is the solution electrical resistance (ohms)). R is in the denominator of the second term. This is a very important equation because, first, the first-order loading rate decreases ("is quenched") with increasing solution electrical conductivity (or decreasing electrical resistance). This equation predicts the response of LANR to an applied magnetic field intensity in an LANR system. If the applied magnetic field

intensity is sufficient, this term may dominate, actually increasing the system performance. Increasing the solution electrical resistance (R) increases LANR loading. The converse, through the second term can end all loading and LANR performance.

Second, in addition, the changes in vectors from the applied magnetic field intensity, with the observed decreased electrophoretic mobility, may be the etiology of some of the morphologies reported by Szpak, Gordon and Mosier-Boss [47,19,41].

6. Conclusion – Possibility of Increased Loading

An applied magnetic field ($\sim$0.3 T) to the high impedance DAP (Dual anode PHUSOR(R) type) LANR system increases the LANR solution's electrical resistance $\sim$10–17% . The time constant for change was on the order of minutes. The incremental resistance increase to an applied H-field is greatest at low input loading and driving electrical currents. The incremental resistance increase to an applied H-field is greatest with the applied H-field perpendicular to the applied driving electrical field (E-field) intensity.

The modified LANR loading rate equation indicates that an applied H-field may increase loading in a LANR system by increasing solution resistance. Our past studies, which examined the impact of laser irradiation on LANR cathodes has taught us that any change of solution electrical resistance will directly impact LANR performances through the modified deuteron loading rate equation.

In this paper, it is shown that if an applied magnetic field intensity is sufficient, especially perpendicular to the applied electric field intensity and at lower electrical driving currents, an increase in system performance is expected from increased loading, resulting from an increase in solution electrical resistance. In the future, we anticipate reporting and discussing the observed and expected findings in LANR systems, with various arrangements of applied magnetic field intensities.

Acknowledgments

The author thanks Gayle Verner for her meticulous help, and Larry Parker Forsley for presenting this lecture, and Jeffrey Tolleson, Alan Weinberg, Alex Frank, Charles Entenmann, John Thompson, Peter Hagelstein, Brian Ahern, Pamela Mosier-Boss, Scott Chubb, Jeffrey Driscoll, Richard Kramer, Michael Staker, Jan Marwan, Steven Olasky, Robert Smith, for their critique, valued ideas, suggestions, and JET Energy, Incorporated and New Energy Foundation for contributing to support this effort. PHUSOR® is a registered trademark of JET Energy Inc.

References

[1] Swartz, M.R. Survey of the Observed Excess Energy and Emissions in Lattice Assisted Nuclear Reactions, *J. Scientific Exploration* 23(4) (2009) 419–436.

[2] Swartz, M.R. Excess Power Gain using High Impedance and Codepositional LANR Devices Monitored by Calorimetry, Heat Flow, and Paired Stirling Engines, *Proceedings of the 14th International Conference onCondensed Matter Nuclear Science and the 14th International Conference on Cold Fusion* (ICCF-14), 10–15 August 2008, Washington, DC, David J. Nagel and Michael E. Melich (eds.), ISBN: 978-0-578-06694-3, 2010, p. 123.

[3] Swartz, M., G. Verner, Excess Heat from Low Electrical Conductivity Heavy Water Spiral-Wound Pd/D_2O/Pt and Pd/D_2O-$PdCl_2$/Pt Devices, Condensed Matter Nuclear Science, *Proceedings of ICCF-10*, (eds.) P.L. Hagelstein, S.Chubb, World Scientific, Singapore, pp. 29–44; 45–54, 2006. ISBN 981-256-564-6.

[4] Swartz, M., Consistency of the Biphasic Nature of Excess Enthalpy in Solid State Anomalous Phenomena with the Quasi-1-Dimensional Model of Isotope Loading into a Material, *Fusion Technol*. **31** (1997) 63–74.

[5] Arata, Y., Y.C. Zhang, Anomalous Production of Gaseous ^{4}He at the Inside of DS-Cathode During D_2-Electrolysis, *Proc. Jpn. Acad. Ser. B* **75** (1999) 281; Arata, Y. Y.C. Zhang, Observation of Anomalous Heat Release and Helium-4 Production from Highly Deuterated Fine Particles, *Jpn. J. Appl. Phys*. **38**(2) (1999) L774; Arata, Y., Y. Zhang, The Establishment of Solid Nuclear Fusion Reactor, *J. High Temp. Soc.* **34**(2) (2008) 85.

[6] Celani, F. et al., Deuteron Electromigration in Thin Pd Wires Coated With Nano-Particles: Evidence for Ultra-Fast Deuterium Loading and Anomalous, Large Thermal Effects, in *ICCF-14 International Conference on Condensed Matter Nuclear Science*, Washington, DC, 2008.

[7] Dardik, I., H. Branover, A. El-Boher, D. Gazit, E. Golbreich, E. Greenspan, A. Kapusta, B. Khachatorov, V. Krakov, S. Lesin, B. Michailovitch, G. Shani, T. Zilov, Intensification of Low Energy Nuclear Reactions Using Superwave Excitation, *Proceedings of the 10th International Conference on Cold Fusion*, Peter L. Hagelstein, Scott, R. Chubb (eds.), World Scientific, NJ, ISBN 981-256-564-6, 2006, p. 61.

[8] Dash, J., D.S. Silver, Surface Studies After Loading Metals With Hydrogen And/Or Deuterium, *13th Conf. CMNS 2007*. Sochi, Russia; Dash, J., S. Miguet, Microanalysis of Pd Cathodes after Electrolysis in Aqueous Acids, *J. New Energy* **1**(1) (1996) 23.

[9] Fleischmann, M., S. Pons, Electrochemically Induced Nuclear Fusion of Deuterium, *J. Electroanal. Chem*. **261** (1989) 301–308, erratum, **263** (1989) 187; M. Fleischmann, S. Pons, Some comments on the paper Analysis of Experiments on Calorimetry of LiOD/D_2O Electrochemical Cells, R.H.Wilson et al., *J. Electroanal. Chem*. **332** (1992) 1*, *J. Electroanal. Chem*. **332** (1992) 33–53, M. Fleischmann, S. Pons, Calorimetry of the Pd-D_2O system: from simplicity via complications to simplicity, *Phys. Lett.* A **176** (1993) 118–129, M. Fleischmann, S. Pons, M. Anderson, L.J. Li, M. Hawkins, Calorimetry of the palladium–deuterium-heavy water System, *Electroanal. Chem*. **287** (1990) 293.

[10] Iwamura, Y., M. Sakano, T. Itoh, Elemental Analysis of Pd Complexes: Effects of D_2 Gas Permeation, *Jpn. J. Appl. Phys*. A **41** (2002) 4642, Iwamura, Y. et al., Observation Of Surface Distribution Of Products By X-Ray Fluorescence Spectrometry During D_2 Gas Permeation Through Pd Complexes, in *The 12th International Conference on Condensed Matter Nuclear Science*. Yokohama, Japan, 2005.

[11] Letts D., D. Cravens, Laser Stimulation of Deuterated Palladium: Past and Present, *Proceedings of the 10th International Conference on Cold Fusion*, Peter L. Hagelstein, Scott, R. Chubb (eds.), World Scientific, NJ, ISBN 981-256-564-6, 2006, pp. 171, 159.

[12] Letts, D., P.L. Hagelstein, Stimulation of Optical Phonons in Deuterated Palladium, in *ICCF-14 International Conference on Condensed Matter Nuclear Science*, Washington, DC, 2008; Letts, D., D. Cravens, P.L. Hagelstein, Thermal Changes in Palladium Deuteride Induced by Laser Beat Frequencies, in *Low-Energy Nuclear Reactions Sourcebook*, J. Marwan, S. Krivit (eds), 2008.

[13] McKubre, M., F. Tanzella, P. Hagelstein, K. Mullican, M. Trevithick, The Need for Triggering in Cold Fusion Reactions, *Proc. 10th International Conf. on Cold Fusion*, Peter L. Hagelstein, Scott, R. Chubb (eds.), World Scientific, NJ, ISBN 981-256-564-6, 2006, p. 199.

[14] Miles, M.H., R.A. Hollins, B.F.Bush, J.J. Lagowski, R.E. Miles, Correlation of excess power and helium production during D_2O and H_2O electrolysis, *J. Electroanal. Chem*. **346** (1993) 99–117.

[15] Miles, M.H., B.F.Bush, Heat and Helium Measurements in Deuterated Palladium, *Trans. Fusion Technol*. **26** (1994) 156–159.

[16] Miles, M.H. et al. Calorimetric Analysis of a Heavy Water Electrolysis Experiment Using a Pd-B Alloy Cathode, Naval Research Laboratory Report NRL/MR/6320-01-8526, pp. 155, March 16, 2001.

[17] Miley, G.H., G. Narne, T. Woo, Use of combined NAA and SIMS analyses for impurity level isotope detection. *J. Radioanal. Nucl. Chem*. **263**(3) (2005) 691–696, Miley, G.H., J. Shrestha, Transmutation Reactions and Associated LENR Effects in Solids, in *Low-Energy Nuclear Reactions Sourcebook*, J. Marwan, S. Krivit (eds.), Oxford University Press, Oxford, 2008.

[18] Mosier-Boss, P.A., S. Szpak, 'The Pd/nH System: Transport Processes and Development of Thermal Instabilities, Il *Nuovo Cimento* **112A** (1999) 577–585.

[19] Mosier-Boss, P.A, S. Szpak, F.E. Gordon, L.P.G. Forsley, Use of CR-39 in Pd/D Co-Deposition Experiments, *Euro. Phys. J.Appl. Phys*. **40** (2007) 293–303.

[20] Mosier-Boss, P.A., S. Szpak, F.Gordon, L.P.Forsley, Triple Tracks in CR-39 Evidence of Energetic Neutrons, *Naturwissenschaften* **96** (2009) 135–142.

[21] Pons, S., Fleischmann, M., Heat After Death, *Proc. ICCF-4*, Maui, EPRI TR104188-V2, vol. 2, 1994, pp. 8–1, *Trans. Fusion Technol.* **26** (4T, Part 2) (1994) 87.

[22] Srinivasan, M. et al., Tritium and Excess Heat Generation During Electrolysis of Aqueous Solutions of Alkali Salts with Nickel Cathode, Frontiers of Cold Fusion, H. Ikegami (ed.), *Proceedings of the Third International Conference on Cold Fusion*, October 21–25, 1992, Universal Academy Press, Tokyo, pp. 123–138.
[23] Stringham, R., Cavitation and Fusion, *ICCF-10*, Cambridge, MA, 2003.
[24] Swartz. M., Can a Pd/D_2O/Pt Device be Made Portable to Demonstrate the Optimal Operating Point?, Condensed Matter Nuclear Science, *Proceedings of ICCF-10*, Peter L. Hagelstein, Scott, R. Chubb (eds.), World Scientific Publishing, NJ, 2006, pp. 29–44; 45–54. ISBN 981-256-564-6.
[25] Swartz, M., Codeposition Of Palladium And Deuterium, *Fusion Technol.* **32** (1997) 126–130.
[26] Swartz, M., Noise Measurement in cold fusion systems, *J. New Energy* **2** (2) (1997) 56–61.
[27] Swartz, M., Patterns of Failure in Cold Fusion Experiments, *Proc. 33RD Intersociety Engineering Conference on Energy Conversion*, IECEC-98-I229, CO, Aug. 1998.
[28] Swartz. M., Patterns of Success in Research Involving Low-Energy Nuclear Reactions, *Infinite Energy* **31** (2000) 46–48.
[29] Swartz. M., The Impact of Heavy Water (D_2O) on Nickel-Light Water LANR Systems, *Proc. of the 9th International Conference on Cold Fusion*, Beijing, China, Xing Z. Li (ed.), pp. 335–342, May 2002.
[30] Swartz, M., G. Verner, Dual Ohmic Controls Improve Understanding of 'Heat after Death, *Trans. Amer. Nucl. Society* **93** (2005) 891–892. ISSN:0003-018X.
[31] M. Swartz, G. Verner, Two Sites of Cold Fusion Reactions Viewed by their Evanescent Tardive Thermal Power, Abstract of ICCF-11, 2004; M. Swartz, Kinetics and Lumped Parameter Model of Excess Tardive Thermal Power, Mitchell Swartz, APS (2005).
[32] Swartz, M., G. Verner, Metamaterial Function of Cathodes Producing Hydrogen Energy and Deuteron Flux, in *ICCF-14 International Conference on Condensed Matter Nuclear Science*, 10–15 August 2008, Washington, DC, David J. Nagel and Michael E. Melich (eds.), ISBN: 978-0-578-06694-3, 2010, p. 458. .
[33] Swartz, M., G. Verner, Photoinduced Excess Heat from Laser-Irradiated Electrically-Polarized Palladium Cathodes in D_2O, Condensed Matter Nuclear Science, *Proc. ICCF-10*, Peter L. Hagelstein, Scott Chubb (eds.), NJ, 2006, pp. 213–226. ISBN 981-256-564-6.
[34] Swartz, M., G.Verner, A.Weinberg, Non-Thermal Near-IR Emission Linked with Excess Power Gain in High Impedance and Codeposition PHUSOR-LANR Devices, in *ICCF-14 International Conference on Condensed Matter Nuclear Science*, 10–15 August 2008, Washington, DC, David J. Nagel and Michael E. Melich (eds.), ISBN: 978-0-578-06694-3, 2010, p. 343.
[35] Swartz, M, Improved Electrolytic Reactor Performance Using pi-Notch System Operation and Gold Anodes, Trans. American Nuclear Association, Nashville, Tenn Meeting, (ISSN:0003-018X publisher LaGrange, Ill) Vol. 78, 1998, pp. 84–85.
[36] Swartz, M.R., Breakeven from LANR PHUSOR Device Systems: Relative Limitations of Thermal Loss in Feedback Loop, in *ICCF-14 International Conference on Condensed Matter Nuclear Science*,D. J. Nagel and M. E. Melich (eds.), 2010.
[37] Swartz, M.R., Excess Heat and Electrical Characteristics of Type B Anode-Plate High Impedance PHUSOR-type LANR Devices, *J. Scientific Exploration*, American Chemical Society, Salt Lake City, UT, 2010, in press.
[38] Szpak S., P.A. Mosier-Boss, 'On the Behavior of the Cathodically Polarized Pd/D System: a Response to Vigier's Comments, *Phys. Letts*. A **221** (1996) 141–143, Szpak S., P.A. Mosier-Boss, S.R. Scharber, J.J. Smith, Cyclic Voltammetry of Pd+D Codeposition, *J. Electroanal. Chem*. **380** (1995) 1–6.
[39] Szpak S., P.A. Mosier-Boss, J.J. Smith, Deuterium Uptake During Pd–D Codeposition, *J. Electroanal. Chem*. **379** (1994) 121–127.
[40] Szpak S., P.A. Mosier-Boss, F.E. Gordon, Further Evidence of Nuclear Reactions in the Pd/D Lattice: Emission of Charged Particles, *Naturwissenschaften* **94** (2007) 511–514.
[41] Szpak S., P.A. Mosier-Boss, C. Young, F.E. Gordon, Evidence of Nuclear Reactions in the Pd Lattice, *Naturwissenschaften* **92** (2005) 394–397.
[42] Szpak S., P.A. Mosier-Boss, S.R. Scharber, J.J. Smith, Charging of the Pd/nH System: Role of the Interphase, *J. Electroanal. Chem*. **337** (1992) 147–163.
[43] Szpak S., P.A. Mosier-Boss, M.H. Miles, M. Fleischmann, Thermal Behavior of Polarized Pd/D Electrodes Prepared by Co-Deposition, *Thermochim. Acta* **410** (2004) 101–107.
[44] Szpak S., P.A. Mosier-Boss, J.J. Smith, On the Behavior of the Cathodically Polarized Pd/D System: Search for Emanating Radiation, *Phys. Letts.* A **210** (1996) 382–390.

[45] Szpak S., P.A. Mosier-Boss, J.J. Smith, On the Behavior of Pd Deposited in the Presence of Evolving Deuterium, *J. Electroanal. Chem.* **302** (1991) 255–260.
[46] Szpak S., P.A. Mosier-Boss, R.D. Boss, J.J. Smith, On the Behavior of the Pd/D System: Evidence for Tritium Production, *Fusion Technol*. **33** (1998) 38–51.
[47] Szpak, S. et al., The effect of an external electric field on surface morphology of codeposited Pd/D films, *J. Electroanal. Chem.* **580** (2005) 284–290.
[48] Violante, V., E. Castagna, C. Sibilia, S. Paoloni, F. Sarto, Analysis of Mi-Hydride Thin Film After Surface Plasmons Generation by Laser Technique, *Proceedings of the 10th International Conference on Cold Fusion*, Peter L. Hagelstein, Scott, R. Chubb (eds.), World Scientific, NJ, ISBN 981-256-564-6, 2006, pp. 405, 421.
[49] Will, F.G., K. Cedzynska, D.C. Linton, Tritium Generation in Palladium Cathodes with High Deuterium Loading, *Trans. Fusion Technol*. **26** (1994) 209–213, Reproducible tritium generation in electrochemical cells employing palladium cathodes with high deuterium loading, *J. Electroanal. Chem.* **360** (1993) 161–176.
[50] Swartz, M, G. Verner, Bremsstrahlung in Hot and Cold Fusion, *J. New Energy* **3**(4) (1999) 90–101.
[51] H. H. Uhlig, *Corrosion and Corrosion Control*, Wiley, New York, 1971.
[52] J. O'M Bockris, A.K.N. Reddy, *Modern Electrochemistry*, Plenum Press, New York, 1970.
[53] Swartz, M., Quasi-One-Dimensional Model of Electrochemical Loading of Isotopic Fuel into a Metal, *Fusion Technol.* **22**(2) (1992) 296–300.
[54] Swartz, M., Isotopic Fuel Loading Coupled to Reactions At an Electrode, *Fusion Technol*. 26(4T) (1994) 74–77.
[55] A. Von Hippel, *Dielectric Materials and Applications*, MIT Press, Cambridge, 1954.
[56] J.R. Melcher, *Continuum Electromechanics*, MIT Press, Cambridge, 1981.
[57] Swartz, M., Generality of Optimal Operating Point Behavior in Low Energy Nuclear Systems, *J. New Energy* **4**(2) 218–228. (1999).
[58] Swartz. M., Dances with Protons - Ferroelectric Inscriptions in Water/Ice Relevant to Cold Fusion and Some Energy Systems, *Infinite Energy* 44 (2002).
[59] A. Von Hippel, D.B. Knoll, W.B. Westphal, Transfer of Protons through 'Pure' Ice 1h Single Crystals, *J. Chem. Phys*. **54** (1971) 134, 145.
[60] Swartz, M.R., Optimal Operating Point Manifolds in Active, Loaded Palladium Linked to Three Distinct Physical Regions, in *ICCF-14 International Conference on Condensed Matter Nuclear Science*, Washington, DC, 2010, in press.
[61] Hampel, C.A., *Rare Metal Handbook*, Reinhold Pub., NY, 1954.
[62] Hansen, M., K. Anderko, *Constitution of Binary Alloys*, McGraw-Hill, NY, 1958.
[63] Swartz. M., Catastrophic Active Medium Hypothesis of Cold Fusion, Fourth International Conference on Cold Fusion, Vol. 4, Sponsored by EPRI and the Office of Naval Research, 1994, Swartz, M., Hydrogen Redistribution By Catastrophic Desorption In Select Transition Metals, *J. New Energy* 1(4) (1997) 26–33.
[64] Papaconstantopoulos, D.A., B.M. Klein et al., Band structure and superconductivity of PdDx and PdHx, *Phys. Rev.* **17**(1) (1977) 141150.
[65] Wicke, E., H. Brodowsky, Hydrogen in Palladium and Palladium Alloys, *Hydrogen in Metals* II, G. Alefield, J. Volkl, (eds.), Springer, Berlin, 1978.
[66] Teichler, H., Theory of hydrogen hopping dynamics including hydrogen-lattice correlations, *J. Less-Common Metals* **172–174** (1991) 548–556.
[67] Klein, B.M., R. E. Cohen, Anharmonicity and the inverse isotope effect in the palladiumhydrogen system, *Phys. Rev*. B **45**(21 (1992) 405.
[68] Swartz, M., US Patent Application 07/339,976, 1989.